Process development for elemental recovery from PGM tailings by thermochemical treatment: Preliminary major element extraction studies using ammonium sulphate as extracting agent

Sameera Mohamed[a,b], Elizabet M. van der Merwe[c], Wladyslaw Altermann[b,†], Frédéric J. Doucet[a,d*]

[a] *Council for Geoscience, Private Bag X112, Pretoria 0001, South Africa.*

[b] *Department of Geology, University of Pretoria, Lynnwood Road, Pretoria 0002, South Africa* ([†] Kumba-Exxaro chair)

[c] *Department of Chemistry, University of Pretoria, Lynnwood Road, Pretoria 0002, South Africa*

[d] *Chemical Resource Beneficiation, North-West University, Private Bag X6001, Potchefstroom 2520, South Africa*

* Corresponding author. Tel: +27 (0) 12 841 1300. E-mail address: fdoucet@geoscience.org.za

Highlights

- PGM tailings represent untapped secondary metal and mineral resources.
- Major elements were extracted from PGM mine tailings.
- Extraction was achieved via thermochemical treatment followed by aqueous leaching.
- The process used ammonium sulphate, a low-cost, recyclable chemical agent.
- Preliminary extraction efficiencies amount to 60% for Al, 80% for Ca and 35% for Fe.

Abstract

Mine tailings can represent untapped secondary resources of non-ferrous, ferrous, precious, rare and trace metals. Continuous research is conducted to identify opportunities for the utilization of these materials. This preliminary study investigated the possibility of extracting major elements from South African tailings associated with the mining of Platinum Group Metals (PGM) at the Two Rivers mine operations. These PGM tailings typically contain four major elements (11% Al_2O_3; 12% MgO; 22% Fe_2O_3; 34% Cr_2O_3), with lesser amounts of SiO_2 (18%) and CaO (2%). Extraction was achieved via thermochemical treatment followed by aqueous dissolution, as an alternative to conventional hydrometallurgical processes. The thermochemical treatment step used ammonium sulphate, a widely available, low-cost, recyclable chemical agent. Quantification of the efficiency of the thermochemical process required the development and optimisation of the dissolution technique. Dissolution in water promoted the formation of secondary iron precipitates, which could be prevented by leaching thermochemically-treated tailings in 0.6M HNO_3 solution. The best extraction efficiencies were achieved for aluminium (ca. 60%) and calcium (ca. 80%). 35% iron and 32% silicon were also extracted, alongside chromium (27%) and magnesium (25%). Thermochemical treatment

using ammonium sulphate may therefore represent a promising technology for extracting valuable elements from PGM tailings, which could be subsequently converted to value-added products. However, it is not element-selective, and major elements were found to compete with the reagent to form water-soluble sulphate-metal species. Extracted aluminium could be used for the production of alumina. Extracted iron could be used by the iron and steel industry or for the synthesis of nano-adsorbents for wastewater remediation. Extracted magnesium could be converted to carbonate for CO_2 mineral sequestration. Further development of this integrated process, which aims at achieving the full potential of utilization of PGM tailings, is currently underway.

Keywords

PGM tailings; ammonium sulphate; metal recovery and extraction; thermochemical treatment; solid-solid reaction

1 Introduction

Numerous countries face economic, environmental and health-related challenges, which are associated with the management of large volumes of solid mine residues (e.g. tailings; Asif and Chen, 2016). This is particularly relevant in South Africa, which is the biggest global producer of platinum, gold and chrome (Mohale et al., 2015). An aspect which is often overlooked in the life cycle of sustainable mine residues management, and which can resolve, at least partly, these challenges, is that mine residues can also represent untapped secondary resources for valuable minerals and metals (Frändegård et al., 2015). For instance, integrated processes are being developed for the recovery of metals from bauxite residue (Liu and Naidu, 2014) and copper tailings (Chmielewski et al., 2016), and for the conversion of bauxite tailings to highly-crystalline zeolites (Ma et al., 2014). Cyanidation tailings have been used to synthesize nano-iron red oxide pigment (Li et al., 2008). Iron ore tailings have served as secondary resource for the synthesis of iron oxide and ultimately magnetic graphene (Muthukannan et al., 2015). Anorthosite tailings have been used for CO_2 mineralization (Ghacham et al., 2015). While the full exploitation of such residues will require a paradigm shift in the field of mine waste management, it also represents one of the central issues of eco-efficient mining in the so-called ‘green mining’ arena, which is already gaining momentum in locations such as Europe, Canada and Australia (Watson et al., 2016). Another aspect of waste valorization, which is emerging as an important area for metal recovery, is ‘landfill mining’ (Gutiérrez et al., 2015; Wagner and Raymond, 2015), a concept whereby “minerals or other solid natural resources contained in waste materials that previously had been disposed of by burying them in the

ground" are extracted for resource recovery (Krook et al., 2012). However, economically successful recovery of minerals and metals from solid mine residues may be less challenging than from landfills, since the latter suffers to a greater extent of insufficient information on its contents in valuable elements, such as concentration, type and location of metal in the landfill site.

South Africa accounts for 96 percent of known global reserves of the platinum group metals (PGMs; Mohale et al., 2015). The country's mining operations associated with the primary production of PGMs from Merensky, Upper Group 2 (UG2) and Platreef operations in the Bushveld Igneous Complex (BIC), generate over 77 Mt of fresh tailings per annum (Vogeli et al., 2011). In 2008, Anglo Platinum had already reported a cumulative 730.8 Mt of generated tailings (Anglo Platinum, 2009). The ever-increasing volumes of piled PGM tailings pose considerable challenges to the mining sector. These alkaline tailings are regarded as hazardous waste, which must be managed properly to avoid contamination to local surface and ground waters. However, these high-tonnage materials generally contain elevated concentrations of iron, aluminium, chromium and magnesium, and low to moderate amounts of titanium and other valuable elements, depending on their origin (Mohamed, 2015). They could therefore be regarded as an economic resource rather than a waste, provided suitable economically-viable processes can be developed. For instance, in 2013, the Two Rivers Platinum Mine, located in South Africa, has commissioned a recovery plant to reprocess its tailings to recover the chromite (Implats, 2015). Tailings from other mining sectors (e.g. chromium, vanadium) within the BIC can also contain valuable elements or minerals. For instance, Jubilee Platinum, a South African platinum-focused mining and exploration company, is busy commissioning the largest PGM beneficiation plant of surface chrome tailings in the country for the production of platinum, palladium, rhodium and gold concentrates using the ConRoast process (Jubilee Platinum, 2015). Although most of the focus has been on the recovery of precious and ferrous metals, the extraction of e.g. non-ferrous metals and minerals from tailings is rapidly emerging as a new research area, mostly owing to environmental considerations associated with active, but also with derelict and ownerless (D&O) mines. An example is the recent interest taken in the CO_2 mineralization potential of PGM tailings, owing to their Mg-rich mineralogy (Doucet, 2011; Vogeli et al., 2011; Meyer et al., 2014). However, this approach can only become feasible and economically viable if it is integrated with the co-recovery of e.g. high-value precious and specialty metals, and low-value major elements that can be converted to value-added products. For instance, elements such as iron could be used by the iron and steel industry (Romão et al., 2012) or as feedstock for the synthesis of nano-based materials for wastewater treatment processing (Gehrke et al., 2015), while aluminium could be used to prepare e.g. alumina (Xiao et al., 2015), and magnesium could be

converted to magnesite ($MgCO_3$) as a CO_2 sequestration mineral technology (Romão et al., 2014). These integrated processes should also achieve high yields, high energy efficiency, minimal emissions, and low volumes of final waste. All these envisaged modes of use of the tailings will significantly reduce the volumes of tailings, and will contribute to the sustainability of the mining sector and to reduction of penalties imposed on mines for waste accumulation.

To date, acid leaching using both strong inorganic (2M HCl) and organic (oxalic acid, EDTA) acids has been shown to be of limited value for cation extraction from PGM tailings, with only up to 3% Mg, 9% Fe and 30% Ca extracted (Meyer et al., 2014). Recently, our group has focused on identifying and testing a potentially promising thermochemical extraction process that makes use of a widely available, low-cost, recyclable chemical agent. Ammonium sulphate salt ($(NH_4)_2SO_4$) meets all three criteria (Highfield et al., 2012). Its thermal solid-solid reactions with silicate (Bayer et al., 1982; Abd-Elzaher, 1999; Nduagu et al., 2012) and oxide (Bayer et al., 1982; Nagaishi et al., 1984; Mudher et al., 1999) minerals for elemental extraction have been extensively studied for over 30 years. In recent years, its reactivity with serpentinite rocks from Finland and other countries has been the focus of great attention at Åbo Akademi University (Finland), primarily in the context of mineral CO_2 sequestration (e.g.Nduagu et al., 2014; Romão et al., 2014, 2015; and references therein). However, the reactivity of silicate and oxide mineral assemblages present in PGM tailings (e.g. orthopyroxene, clinopyroxene, anorthite) with $(NH_4)_2SO_4$ for cation extraction has yet to be elucidated.

The primary objective of this paper was to introduce this alternative multi-stage extraction process, and to report on the results of our preliminary major element extraction study, using the Two Rivers PGM mine tailings as a case study. An outline of the multi-stage extraction process is illustrated in Figure 1. Quantification of the efficiency of the thermochemical step was achieved by developing and using an optimized dissolution step. This paper will later be followed by a comparison of results obtained with different ammonium salts ($(NH_4)_2SO_4$ vs NH_4NO_3 vs NH_4Cl). A third paper will look at major element extraction from PGM tailings with varying Cr content using $(NH_4)_2SO_4$.

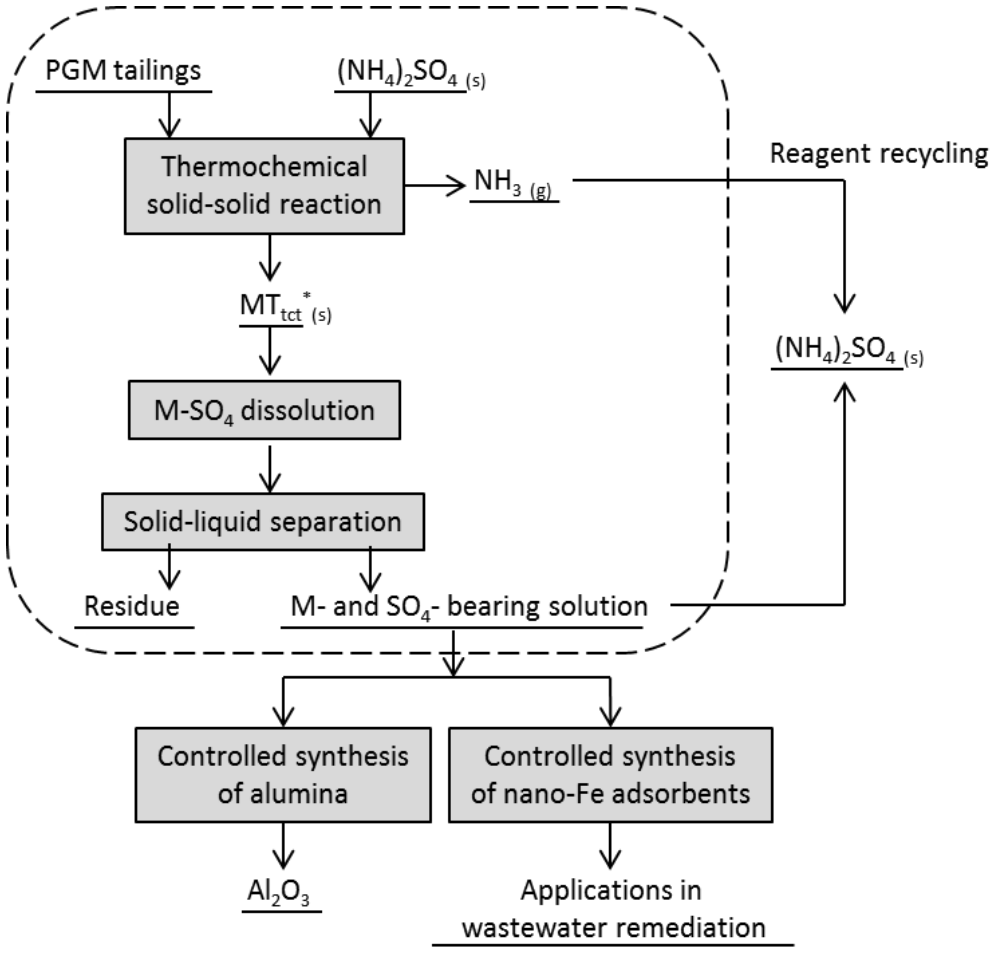

Figure 1. Process flow diagram for the multi-stage extraction of major elements from PGM mine tailings (* MT_{tct} contains M-SO_4 compounds, where M is a metal; the highlighted area represents the focus of this study).

2 Experimental approach

2.1. Material tested

A sample of platinum mine tailings was collected from the Two Rivers platinum mine located in the southern sector of the eastern limb of the BIC, in the province of Mpumalanga, South Africa (GPS coordinates: 24°57'03 S and 30°06'20 E). At this site, mining of PGMs occurs in the UG2 chromitite and Merensky Reef, which comprise the Critical Zone of the BIC, and which is rich in platinum-bearing ore-bodies. The critical zone is an 800m vertical succession of alternating cyclical rock units of chromitite, and pyroxenite, norite and anorthosite, comprising disseminated chromite (Cawthorn *et al.*, 2006; Eales, 2014). The diagnostic mineral phases include orthopyroxene, plagioclase, chromite and olivine.

Deposition of the tailings occurs via the jet method, which causes fractionation of the particles whereby coarser particles are deposited on the bank and the finer particles are found within the dam itself (African Rainbow Minerals, 2013; Huisamen, 2013). About 200kg of PGM mine tailings (MT) were collected from the top of the tailings dam, using the grab sampling technique. No attempt was made to have a representative sample of the tailings dam at this stage. Immediately upon arrival at the laboratory, the sample was air-dried up to constant weight. Homogeneous sub-samples were obtained using a sample splitter for future experiments. A sub-sample (MT_{bulk}) was selected and particle size analysis was performed using laser diffraction (Malvern Mastersizer 2000 fitted with a Hydro 2000G dispersion unit, Malvern Instrument Ltd., Worcester, UK). One particle size fraction, 45-75 µm (hereafter called MT_{45-75}), was obtained by sieving and was used for the tests reported here.

2.2. Preliminary thermochemical treatment (static furnace)

MT_{45-75} was mixed thoroughly with ammonium sulphate ($(NH_4)_2SO_4$; reagent grade, 99.5%, Merck, South Africa) at a constant solid-solid mass ratio of 2:6 (m/m). As reported previously (Nduagu et al., 2012), mixing two solids (MT_{45-75} and $(NH_4)_2SO_4$) with distinct physical properties (*e.g.* particle size) can be challenging and the preparation of homogeneous mixtures cannot be assured. However, the same method was applied to all experiments and good reproducibility was confirmed. Grinding MT_{45-75}-$(NH_4)_2SO_4$ mixtures, or $(NH_4)_2SO_4$ on its own, using a mortar and pestle helped to produce homogeneous mixtures. It also increased the specific surface area per unit mass of $(NH_4)_2SO_4$ particles, which was expected to improve its reactivity with MT_{45-75}. However, it also caused accelerated thermal decomposition of finely ground $(NH_4)_2SO_4$ during thermochemical treatment, compared to that of the supplied coarser particles, which had a negative effect on the elemental extraction efficiency. The resulting mixtures (unground) were placed in fused quartz crucibles and were subsequently heat-treated in a muffle furnace set at varying temperatures (350, 400, 450, 500 or 550°C) for 45 min. The products of the reaction (hereafter denoted MT_{tct}) were allowed to cool down to 25°C and were ground using a mortar and pestle before characterization and subsequent treatment.

2.3. Optimisation of dissolution procedure

The thermochemical process was anticipated to induce mineral transformations within MT_{45-75}, in particular the formation of water-soluble metal sulphate species. Quantification of the efficiency of

the process could only be achieved by subjecting MT_{tct} to an optimal dissolution procedure to enable complete metal extraction from formed sulphate species. Optimal dissolution is also critical for ensuring the effective recovery of ammonium sulphate with minimal loss. For this purpose, and based on mineralogical information collected on MT_{tct} generated during the preliminary experiment (section 3.2), MT_{tct} obtained via thermochemical treatment of $MT_{45\text{-}75}$ at 550°C was selected as starting material for optimization of the dissolution procedure.

All dissolution experiments were performed in closed high-density polyethylene bottles. Untreated $MT_{45\text{-}75}$ (control) and MT_{tct} (3.00 ± 0.02 g; dry weight) were dispersed in 500 ml of either ultra-pure water (electrical conductivity < 1 µS cm^{-1}) or 0.63M HNO_3 solution. All control and treatment solutions were continuously stirred at a constant speed of 850 rpm, using a mechanical overhead stirrer (WiseStir HS30D, Wisd Lab Instruments) fitted with a 50 mm^3 bladed propeller-type impeller to maintain the particles in suspension throughout the experiments. Dissolution in ultra-pure water was performed at 25°C and at 80°C during periods of time ranging from 30 min up to 64 h, whereas acidic dissolution was studied at several temperatures (25, 60, 80, and 95°C) between 4 and 17 h. At the end of the experiments, the leachates were filtered under reduced pressure through 0.4 µm membrane filters (Whatman Nucleopore® Track-Etched polycarbonate, Whatman UK Ltd.) in closed polycarbonate filtration vessels (Sterifil, 47 mm Millipore). The filtrates were acidified below pH 2 (when necessary) and were subsequently analysed for their content in major elements by inductively coupled plasma optical emission spectrometry (ICP-OES) at an accredited laboratory (Waterlab Pty Ltd, Pretoria, South Africa). These ICP data were used to calculate elemental extraction efficiencies, *i.e.* the mass fraction of elements (especially Al, Ca, Cr, Fe, Mg and Si) extracted as sulphates from the mass of these elements present in $MT_{45\text{-}75}$. The non-dissolved residues (MT_{res}) were rinsed thoroughly with ultra-pure water, oven-dried at 40 °C up to constant weight, and characterized by XRD and TGA. Progress of the dissolution reactions performed in ultra-pure water was monitored by measuring the solution pH and electrical conductivity (Hanna HI 2829 multi-parameter logger) as leaching progressed. Under acidic conditions, the presence of HNO_3 caused the solution conductivity to be greater than the maximum permissible measuring range of the logger (*i.e.* > 200 mS cm^{-1}). Progress of these reactions using the logger could therefore not be monitored over time.

2.4. Characterisation of solid materials

Chemical and mineralogical compositions of $MT_{45\text{-}75}$ were obtained using XRF (PANanalytical Axios X-ray fluorescence spectrometer equipped with a 4 kW Rh tube) and XRD (Bruker D8 Advance X-ray

diffractometer), respectively. The untreated samples were micronized to a particle size < 30 µm for increased accuracy prior to XRD analysis. Phase concentrations were determined by Rietveld quantitative analysis with DIFFRAC.TOPAS software with accuracy in the region of ± 1%.

TGA analyses were performed on a Mettler Toledo TGA/SDTA851e Thermogravimetric Analyzer. Approximately 20 mg of sample was placed in an alumina pan and heated from 25 to 1000^{o}C at a heating rate of 10^{o}C/min. Thereafter, the sample was kept isothermally at 1000^{o}C for 10 min. Air was used as the purge gas at a flow rate of 60 ml/min.

Field-emission scanning electron micrographs (FE-SEM) were collected using a Gemini® Ultra Plus Field Emission microscope (Carl Zeiss, Germany) operating under high-vacuum condition with an accelerating voltage of 1.0 kV to obtain information on morphologies and size distribution of all solid materials. Samples were mounted on a metal substrate by means of a double-sided carbon tape and subsequently sputter-coated with a thin, conductive layer of carbon using an Emitech K550X coater (Ashford, England).

3 Results and discussion

3.1. Materials characterization

PGM-bearing particles are typically characterised by an average size of approximately 12 µm, and rarely exceeds 30 µm (Schouwstra and Kinloch, 2000). For this reason, the ore (Merensky, UG2 and Platreef) is subjected to a rigorous comminution exercise which achieves efficient liberation and recovery of the valuable materials. Process tailings resulting from this practice are therefore composed of finely-grained particles, with reported $D(v,0.5)$ values in the range 22-66 µm and $D(v,0.9)$ values lower than 250 µm (*e.g.* Northam and BRPM Platinum operations located along the Western limb of BIC; Vogeli et al., 2011). In this study, the bulk sample collected at Two Rivers mine contained coarser particles and was characterised by a mean diameter $D(v,0.5)$ of 131.4 µm, with 10% and 90% of the particles being smaller than 26.4 and 328.7 µm respectively. Variation in particle size between tailings from different operations was also reported for Impala, Union, Mogalakwena, Rustenburg Section and Amandelbult PGM mines (Amponsah-Dacosta and Reid, 2014). This variation in grain size between tailings from different mines may be due to several factors, such as the use of various comminution techniques, variation in the intrinsic mineralogical character of mined ore, and heterogeneity of tailings dams.

Table 1. Mineralogical composition of the 45-75 µm fraction of untreated Two Rivers platinum mine tailings (M_{45-75}).

Mineral group (mineral)	Ideal chemical composition	Abundance (%)
Spinel group minerals[a] (magnetite + chromite+ulvöspinel)	$Fe^{2+}O.Fe^{3+}{}_2O_3$ + $(Mg,Fe)O.(Cr,Al,Fe)_2O_3$ + $Fe^{2+}O.(Fe^{2+}Ti^{4+})O_3$	29.5
Orthopyroxene, mostly enstatite	$Mg_2Si_2O_6$	27.8
Plagioclase (anorthite)	$Ca(Al_2Si_2O_8)$	25.2
Amphibole (Hornblende)	$Ca_2[Mg_4(Al,Fe^{3+})]Si_7AlO_{22}(OH)_2$	7.9
Chlorite	$(Mg_5Al)(Si,Al)_4O_{10}(OH)_8$	3.1
Calcite	$CaCO_3$	2.4
Clinopyroxene (Augite)	$(Ca,Mg,Fe)_2Si_2O_6$	1.7
Mica (Biotite)	$KFeMg_2(AlSi_3O_{10})(OH)_2$	1.6
Clay (Talc)	$Mg_3Si_4O_{10}(OH)_2$	1.0
Serpentine (lizardite)	$Mg_3Si_2O_5(OH)_4$	trace

[a] Minerals of the spinel group are traditionally known as oxides with the generic formula AB_2O_4, where the symbols A and B represent divalent (e.g. Fe^{2+}, Mg^{2+}, Mn^{2+}, Ni^{2+} or Zn^{2+}) and trivalent ions (Fe^{3+}, Al^{3+}, Cr^{3+} or the pair $(Fe^{2+}Ti^{4+})^{6+}$ respectively. Only three species are relevant to the Bushveld Complex: magnetite ($Fe^{2+}O.Fe^{3+}{}_2O_3$), chromite ($(Mg,Fe)O.(Cr,Al,Fe)_2O_3$) and ulvöspinel ($Fe^{2+}O.(Fe^{2+}Ti^{4+})O_3$) (Eales, 2014).

XRD of untreated MT_{45-75} revealed the complexity of its mineralogy (Table 1), which represents a combination of the mineralogical composition of both UG2 and Merensky Reefs. Its composition was dominated by spinel group minerals (29.5%; most probably chromite, magnetite and ulvöspinel in varying proportions; Eales, 2014), orthopyroxene (27.8%; mostly enstatite) and plagioclase (25.2%). The tailings sample also contained amphibole (7.9%), and several alteration minerals, namely chlorite (3.1%), talc (1.0%) and serpentine (trace), albeit in much smaller proportions. Minor primary minerals included clinopyroxene (1.7%) and mica (1.6%). The complex mineralogy and the occurrence of elevated chromite spinel content in the UG2 reef horizon were confirmed elsewhere (Rule, 2008). The abundance of spinel group minerals in the sample helped to explain the moderate amount of SiO_2 (17.4%) and the elevated amounts of Cr_2O_3 (31.9%) and $Fe_2O_{3(tot)}$ (23.3%) reported by XRF (Table 2). Al_2O_3 (12.2%) and MgO (13.6%) were also present in significant amount, with plagioclase and chromite contributing to most of Al_2O_3, and with most of MgO being confined to the orthopyroxene component. The sample exhibited a slightly negative loss on ignition (LOI = -1.3; Table 2). This characteristic suggested the probable occurrence of a weight increase arising from the oxidation of ferrous iron (Fe^{2+}) contained in e.g. spinel group minerals to ferric ion (Fe^{3+}), which would have been higher than the weight loss caused by removing volatiles from the mineral structures. Similar observations were already made (i) for iron-rich coal ashes, in which case negative LOI was also best explained by the oxidation of Fe^{2+} to Fe^{3+} (FeO to Fe_2O_3) and its associated

weight increase (Vandenberghe et al., 2010), and (ii) for calcium sulphide (CaS)-rich samples which exhibited a negative LOI due to the oxidation of CaS to $CaSO_4$ (de Beer et al., 2014).

Table 2. Chemical composition of the 45-75 μm fraction of untreated Two Rivers platinum mine tailings (M_{45-75}).

	Concentration (wt. %)[a]							
	SiO_2	Al_2O_3	$Fe_2O_{3(tot)}$	Cr_2O_3	MgO	MnO	CaO	LOI[b]
MT_{45-75}	17.4	12.2	23.3	31.9	13.6	0.3	2.5	-1.3

[a] Other elements present in small amounts: Na_2O (0.3%); K_2O (0.1%); TiO_2 (0.7%).

[b] Loss on ignition.

3.2. Thermal decomposition of ammonium sulphate

In order to better understand the process of thermochemical treatment of PGM tailings with $(NH_4)_2SO_4$, it is important to gain insight on the thermal decomposition of pure $(NH_4)_2SO_4$ over the temperature range studied since it will affect the thermochemical process. The published literature revealed disagreement as to the nature of the intermediate species formed during thermal decomposition of ammonium sulphate. Nevertheless, a general consensus (Lee et al., 1989; Jariwala et al., 2007; Nduagu et al., 2014; and references therein) is that the decomposition mechanism may involve the following main stages:

$$T \approx 300^oC:\ 2(NH_4)_2SO_4(s) \rightarrow (NH_4)_3H(SO_4)_2(s) + NH_3(g) \quad (1)$$

$$T \approx 300^oC:\ (NH_4)_2SO_4(s) \rightarrow NH_4HSO_4(s) + NH_3(g) \quad (2)$$

$$T \approx 300^oC:\ (NH_4)_2SO_4(s) + NH_4HSO_4(s) \rightarrow (NH_4)_3H(SO_4)_2(s) \quad (3)$$

$$T \approx 400^oC:\ 3(NH_4)_3H(SO_4)_2(s) \rightarrow 3(NH_4)_2S_2O_7(s) + 3\,NH_3(g) + 3H_2O(g) \quad (4)$$

$$T \approx 400^oC:\ 3(NH_4)_2S_2O_7(s) \rightarrow 2\,NH_3(g) + 6SO_2(g) + 9H_2O(g) + 2N_2(g) \quad (5)$$

$$3(NH_4)_2SO_4(s) \rightarrow 4\,NH_3(g) + 3SO_2(g) + 6H_2O(g) + N_2(g) \quad (6)$$

Jariwala (2007) confirmed the thermal decomposition of $(NH_4)_2SO_4$ to ammonium bisulphate (NH_4HSO_4) at temperatures exceeding the melting point of NH_4HSO_4 (i.e. higher than 180°C), and suggested that $(NH_4)_2SO_4$ may be immediately converted to ammonium pyrosulphate ($(NH_4)_2S_2O_7$)

with a subsequent loss of water. This reaction is reversible, and therefore NH_4HSO_4 can form upon reaction of $(NH_4)_2S_2O_7$ with water.

Other authors (Dixon, 1944; Kiyoura, 1970) reported the possible formation of sulphamic acid (NH_2SO_3H) as intermediate during $(NH_4)_2SO_4$ decomposition, with subsequent formation of $(NH_4)_2S_2O_7$. Kiyoura (1970) described the formation of NH_2SO_3H to occur from 170°C according to:

T<170 °C $\quad 2(NH_4)_2SO_4\,(s) \rightarrow (NH_4)_3H(SO_4)_2\,(s) + NH_3\,(g)$ (7)

T>170 °C $\quad (NH_4)_2SO_4\,(s) \rightarrow NH_4HSO_4\,(s) + NH_3\,(g)$ (8)

$\quad NH_4HSO_4\,(s) \leftrightarrow NH_2SO_3H\,(s) + H_2O\,(g)$ (9)

These authors described NH_2SO_3H to melt around 205°C with subsequent decomposition into hydrogen, ammonia and sulphur dioxide. They also reported the formation of $(NH_4)_2S_2O_7$ via decomposition of NH_4HSO_4 and the reaction between NH_2SO_3H and $(NH_4)_2SO_4$:

$NH_2SO_3H(s) + NH_4HSO_4(s) \rightarrow (NH_4)_2S_2O_7(s)$ (10)

$2\,NH_4HSO_4\,(s) \leftrightarrow (NH_4)_2S_2O_7\,(s) + H_2O\,(g)$ (11)

The decomposition of NH_4HSO_4 into $(NH_4)_2S_2O_7$ (eq (11)) and formation of NH_2SO_3H from $(NH_4)_2SO_4$ (eqs (8) and (9)) was recently further confirmed (Nduago et al., 2014).

The TGA and DTA curves obtained for the decomposition of pure $(NH_4)_2SO_4$ (Figure 2) showed distinct weight losses and endothermic peaks in the temperature range 200 - 350^{o}C (21.6%), 350 - 470^{o}C (75.2%), and a number of small weight loss transitions above 500^{o}C (2.3%). Only two weight loss transitions could be identified in the region 200 - 500ºC from the TGA result, but the DTA curve indicated the occurrence of at least four different transitions in the same temperature range.

Characterisation of these transitions may be studied with the aid of complementary techniques (TGA-FTIR, TGA-MS or TGA-GC) but falls outside the scope of this paper.

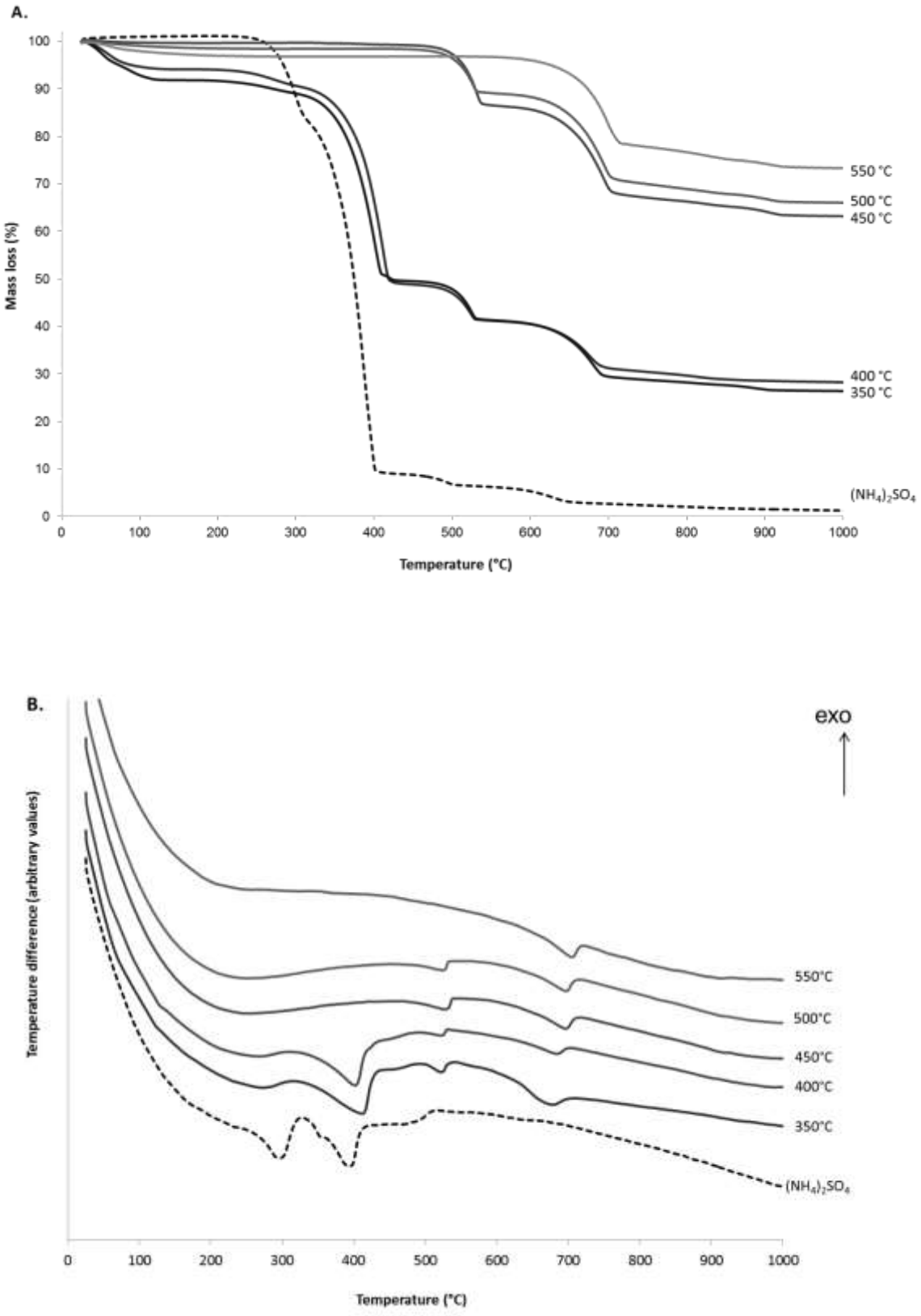

Figure 2. TGA (A) and DTA (B) curves of $(NH_4)_2SO_4$, and of MT_{tct} generated via thermochemical treatment of $MT_{45\text{-}75}$ with $(NH_4)_2SO_4$ at different temperature conditions.

3.3. Preliminary thermochemical treatment (static furnace)

Thermochemical treatment of MT_{45-75} using $(NH_4)_2SO_4$ was investigated under varying temperature conditions to circumscribe the mineralogical changes taking place and at which temperature they occur. The purpose of this qualitative assessment was to select a treatment temperature, for the development and optimization of the subsequent dissolution step. This approach was critical since an optimal dissolution process is required to assess the efficiency of the thermochemical treatment.

Table 3. Percentage mass loss of MT_{45-75} –$(NH_4)_2SO_4$ mixtures following thermochemical treatment ($MT_{45-75:}$ $(NH_4)_2SO_4$ of 2:6; 45 minutes) between 350 °C and 550 °C (*n* = 4).

	Temperature of thermochemical treatment (^oC)				
	350	**400**	**450**	**500**	**550**
Mass loss (%)	14.3 ± 1.3	28.9 ± 0.7	59.9 ± 0.3	62.2 ± 0.5	66.3 ± 0.2

The physical properties of thermochemically-treated MT_{45-75} (MT_{tct}) were strongly influenced by temperature. At elevated temperatures (≥ 450^{o}C), the mass loss incurred by MT_{45-75} – $(NH_4)_2SO_4$ mixtures following treatment ranged from 59.9 to 66.3% (Table 3) and MT_{tct} were free-flowing powders that were easily recovered. In contrast, the mass losses obtained at temperatures ≤ 400^{o}C were found to decrease significantly with temperature and to be as low as 14.3% (Table 3). Under these conditions (i.e. ≤ 400^{o}C), MT_{tct} displayed a molten, viscous-like appearance when hot, i.e. immediately upon removal from the furnace. Upon cooling, these reaction products hardened to resemble solid glassy blocks, which had 'fused' to the walls of the crucible; this made the recovery process of the products challenging. A similar observation was made previously by others, where the authors described the reaction products from the thermochemical treatment of serpentinite with $(NH_4)_2SO_4$ as having the appearance of sintered solid (Nduagu et al., 2012), although they did not report on temperature dependence. The sintered-like appearance and hardness of MT_{tct} produced at lower temperatures combined to the low mass loss obtained under these conditions were best explained by the presence of $(NH_4)_2SO_4$ and/or its decomposition products which had not reacted with MT_{45-75} and/or volatilised within the timeframe of the experiments. This interpretation was further confirmed by XRD, which indicated the prevalence of ammonium bisulphate at temperatures ≤ 400^{o}C (NH_4HSO_4; Table 4). This decomposition product was not identified at higher temperatures.

Table 4. List of newly-formed minerals present in the 45-75 µm fraction of Two Rivers platinum mine tailings following thermochemical treatment ($MT_{45\text{-}75}$: $(NH_4)_2SO_4$ of 2:6; 45 minutes) between 350 °C and 550 °C.

	MT_{act}[a]				
	350°C	**400°C**	**450°C**	**500°C**	**550°C**
Iron sulphate[b]				X	XX
Chromium sulphate[b]				X	X
Iron sulphate hydrate[b]			X	X	X
Ammonium aluminium sulphate[b]		XX	XX	XX	X
Ammonium magnesium sulphate hydrate[b]		X			
Ammonium chromium sulphate[b]					trace
Ammonium chromium sulphate hydrate[b]	X				
Ammonium iron sulphate hydrate[b]	XX	X			
Unidentified species	X	X	X	X	X
Ammonium bisulphate (NH_4HSO_4 (s))	XX	XX			

[a] One cross (X) and two crosses (XX) were arbitrary used to provide a qualitative appreciation of the abundance of new-formed minerals present in the samples (the greater the number of crosses, the most abundant the minerals).

[b] The exact chemical compositions of formed species could not be unambiguously identified strictly on the basis of XRD data.

The range of newly-formed minerals present in MT_{tct} produced at temperatures ≤ 500°C was dominated by intermediate double salts, i.e. ammonium-metal sulphate-based compounds (NH_4^+-*M*-SO_4^{2-}) (Table 4). This was the first indication of the occurrence of a reaction between $(NH_4)_2SO_4$ and some of the mineral phases present in PGM mine tailings. In contrast, far less intermediate phases were identified in MT_{tct} generated at 550°C. At this temperature, the samples were dominated by iron sulphate ($Fe_2(SO_4)_3$; identified as the mineral 'mikasaite' by the XRD database). $Fe_2(SO_4)_3$ was also identified in the sample generated at 500°C, but it represented a much smaller proportion of the sample than at 550°C. It was not identified in samples generated at lower temperatures. These findings suggested that a temperature of 550°C may have facilitated the extraction of Fe to a greater extent than lower temperatures during the timeframe of these experiments. However, thermochemical treatment at lower temperatures and for longer periods of time may improve elemental extractions, as it would minimize/retard the loss of flux due to thermal decomposition (Highfield et al., 2012). The co-existence of chromium sulphate, $Cr_2(SO_4)_3$, and ammonium aluminium sulphate ($NH_4Al(SO_4)_2$), with $Fe_2(SO_4)_3$ in the samples generated at 550°C also suggested the possible occurrence of competitive chemical reactions between Fe, Al and Cr for $(NH_4)_2SO_4$ during thermochemical treatment.

Thermal decomposition of untreated $MT_{45\text{-}75}$ and of MT_{tct} samples was examined using TGA/DTA (Figure 2) to complement the XRD data. The thermogram of untreated $MT_{45\text{-}75}$ was mostly constant, with no distinctive events identified over the duration of the heating program (Figure S1). This

indicated that the mineral phases present in MT_{45-75} had been thermally stable up to 1000^{o}C. A slight mass gain (1.6%) was nevertheless observed, which correlates well with the negative LOI value discussed earlier, and which may therefore be attributed to the oxidation of Fe. The TGA curves (Figure 2A) indicated differences in mass loss between sample, while the DTA curves (Figure 2B) illustrated differences in the energy changes accompanying the decomposition mechanisms of the different mineral phases contained in the samples. The curves showed that the thermal decomposition occurred in several steps. The first step corresponds to the liberation of water, which was completed below 200^{o}C. This was observed for all MT_{tct} samples, but not for $(NH_4)_2SO_4$ or untreated MT_{45-75}. MT_{tct} produced at 350 °C and 400 °C in the furnace exhibited a higher degree of hydration (5.3-7.2%) than MT_{tct} produced at higher temperatures (0.3-2.1%; 450 °C and 550 °C). This was in agreement with the presence of hygroscopic NH_4HSO_4 particles and/or metal sulphate hydrate species in MT_{tct} generated at temperatures ≤ 400^{o}C (Table 4). The presence of ammonium bisulphate in MT_{tct} formed ≤ 400^{o}C was indicated by the loss of NH_3 between 350 °C and 400 °C (Bayer et al., 1982; Nagaishi et al., 1984; also indicated by the endothermic peaks in the present study; Figure 2B), followed by dissociation of ammonium metal sulphate phases from 450 °C and then of metal-sulphate phases from 550°C (Bayer et al., 1982; Nagaishi et al., 1984; Tagawa, 1984). The onset of decomposition of iron, chromium and aluminium sulphates occurs at temperatures ranging between 500-600 °C (Bayer et al., 1982; Krouse et al., 1991; Tagawa, 1984), while that of magnesium sulphate is from 850 °C (Tagawa, 1984). MT_{tct} formed at 550 °C contained very little, if any, NH_3, as confirmed by the absence of mass loss (TGA) and by endothermic peaks (DTA) between 350 °C – 400 °C. For these samples, only the dissociation of metal-sulphate phases was observed above 550 °C. In some of the MT_{tct} products, minor loss of mass was observed around 850 – 900 °C, possibly indicating the presence of $MgSO_4$ in quantities below the detection limit of XRD. Ammonium magnesium sulphate hydrate was observed in MT_{tct} generated at 400^{o}C.

3.4. Dissolution experiments

Extraction of major elements (Fe, Al, Mg, Ca, Si) from MT_{tct} generated at 550^{o}C was evaluated under two leaching environments: (1) H_2O and (2) 0.63M HNO_3.

3.4.1. Dissolution in ultra-pure water

Baseline dissolution experiments were initially conducted in an attempt to assess and compare the dissolution behaviour of untreated MT_{45-75} (control 1) *vs* thermally-treated MT_{45-75} (MT_{ht}; control 2)

vs thermochemically-treated MT_{45-75} (MT_{tct}; treatment). For this purpose, dissolution experiments were conducted in ultra-pure water at 25°C for 6 hours. Dissolution of the two control samples was minimal (Table 5). In particular, the leachates exhibited identical, circumneutral pH values (pH 6.8) and low electrical conductivity (EC < 30 µS/cm). The mass loss sustained by the two starting solid materials following dissolution was also identically low (< 3%). No (Al, Cr, Fe) or little (Ca, Mg) major elements were released to solution during this period (Table 6). In contrast, the leachates obtained from MT_{tct} dissolution displayed acidic pH (pH 3.4) and higher EC values (ca. 600 µS/cm). The mass loss sustained by the sample following dissolution was also greater (ca. 23%). Major elemental extraction efficiency increased slightly (up to 2%) for all elements (except for Ca which remained constant, and for Mg which increased to ca. 8%), although it had remained low. These results were

Table 5. Differences in solution pH and electrical conductivity (EC), and in % mass loss following dissolution of untreated MT_{45-75} (control 1) *vs* thermally treated MT_{45-75} (MT_{ht}; 550 °C; 45 minutes; *n*=2; control 2) *vs* thermochemically treated MT_{45-75} (MT_{tct}; treatment) in ultra-pure water for 6 h (3 g/500 ml; 25°C; 850 rpm; *n*=2).

	pH	EC (µS/cm)	Mass loss (%)
untreated (MT_{45-75})	6.8 ± 0.0	27.5 ± 0.7	2.9 ± 0.0
Thermally-treated (MT_{ht})	6.8 ± 0.1	29.0 ± 1.4	2.9 ± 0.0
Thermochemically-treated (MT_{tct})	3.4 ± 0.1	594.5 ± 75.7	23.3 ± 13.7

Table 6. Concentrations of dissolved elements (mg/l) and corresponding elemental extraction efficiency (%) following dissolution of untreated MT_{45-75} (Control 1) *vs* thermally treated MT_{45-75} (MT_{ht}; 550 °C; 45 minutes; *n*=2; control 2) *vs* thermochemically treated MT_{45-75} (MT_{tct}; MT_{45-75} : AS of 2:6; 550 °C; 45 minutes; *n*=2; Treatment) in ultra-pure water for 6 h (3 g/500 ml; 25°C; 850 rpm; *n*=2).

		Al	Ca	Cr	Fe	Mg
untreated (MT_{45-75})	mg/l	0.1 ± 0.0	2.8 ±1.3	0.0 ± 0.0	0.1 ± 0.1	2.1 ± 0.0
	%	0.0 ± 0.0	4.0 ± 1.9	0.0 ± 0.0	0.0 ± 0.0	0.6 ± 0.0
Thermally-treated (MT_{ht})	mg/l	0.1 ± 0.0	3.5 ± 0.0	0.0 ± 0.0	0.0 ± 0.0	2.1 ± 0.0
	%	0.0 ± 0.0	4.9 ± 0.0	0.0 ± 0.0	0.0± 0.0	0.6 ± 0.0
Thermochemically-treated (MT_{tct})	mg/l	7.9 ± 1.7	5.8 ± 4.0	6.2 ± 0.9	2.7 ± 0.4	47.3 ± 8.2
	%	1.7 ± 0.4	4.0 ± 0.5	0.9 ± 0.2	0.4 ± 0.1	8.2 ± 1.0

somewhat surprising, given that XRD and TGA had confirmed the occurrence of water-soluble ammonium-metal sulphate- and metal sulphate-based compounds in adequate proportions in the thermochemically-treated sample, and Nduagu et al. (2012) reported good elemental extraction efficiencies from a thermochemically-treated Finnish serpentine using the same dissolution conditions.

Clarification on these results was provided by the collection of time-series pH and EC data for solutions during dissolution in ultra-pure water at 25°C (Figure 3A) and at 80°C (Figure 3B) during periods of up to 64h. Upon immersing MT_{tct} in ultra-pure water at 25°C, the solution pH decreased rapidly to 3.5 within 1 min and stabilized at about 2.9 after 17 hours. These pH values were higher than those typically observed for thermochemically-treated serpentine-bearing rock (1.5-2.5; Romão et al., 2015). Concurrently EC increased rapidly from <1 µS cm^{-1} to 400 µS cm^{-1} within 1 min and continued to increase over time before stabilizing at 755 µS cm^{-1} after 17 hours (Figure 3A). Increasing the dissolution temperature from 25 to 80°C resulted in a lower pH (< 2.4) and higher EC (> 2200 µS cm^{-1}) within a short period of time (ca. 3 min; Figure 3B). However, it also gave a different time-series data profile for the two parameters, in particular for EC. Instead of continuously increasing over a 17h-period as observed at 25°C (Figure 3A), EC reached a plateau at 3600-3800 µS cm^{-1} within 2h, which was maintained for approximately 8h, after which EC decreased gradually and reached about 2900 µS cm^{-1} after 64h (Figure 3B). The progressive increase in EC could be ascribed to the dissolution of elements present in MT_{tct}, while the decrease in EC after 10h was a first indication that secondary mineral precipitation had occurred. The occurrence of secondary mineral precipitation was also supported by elemental Fe extraction data (Figures 4A1 and 4A2). More specifically, EC and the concentration of dissolved Fe exhibited similarly-shaped profiles, with the two parameters having reached their maxima after 2h of reaction before having decreased substantially (Figures 3B, 4A and 4B). In contrast to the EC maxima value which had been maintained for several hours, the concentration of dissolved Fe did not reach a plateau, but dropped progressively from its maxima at 23 mg/l before stabilizing at 4 mg/l. This slight difference in the profile of the two parameters was best explained by the solution behaviour of other major elements present in MT_{tct} during the dissolution step, which did not reprecipitate and which therefore continued contributing to the evolution of EC throughout the experiment. The occurrence of secondary precipitation was lastly further confirmed by the colour change of the suspensions. The change in colour followed a continuum from murky green to yellowish brown, light brown and finally dark brown, as the dissolution reaction unfolded. The brown precipitate obtained following filtration

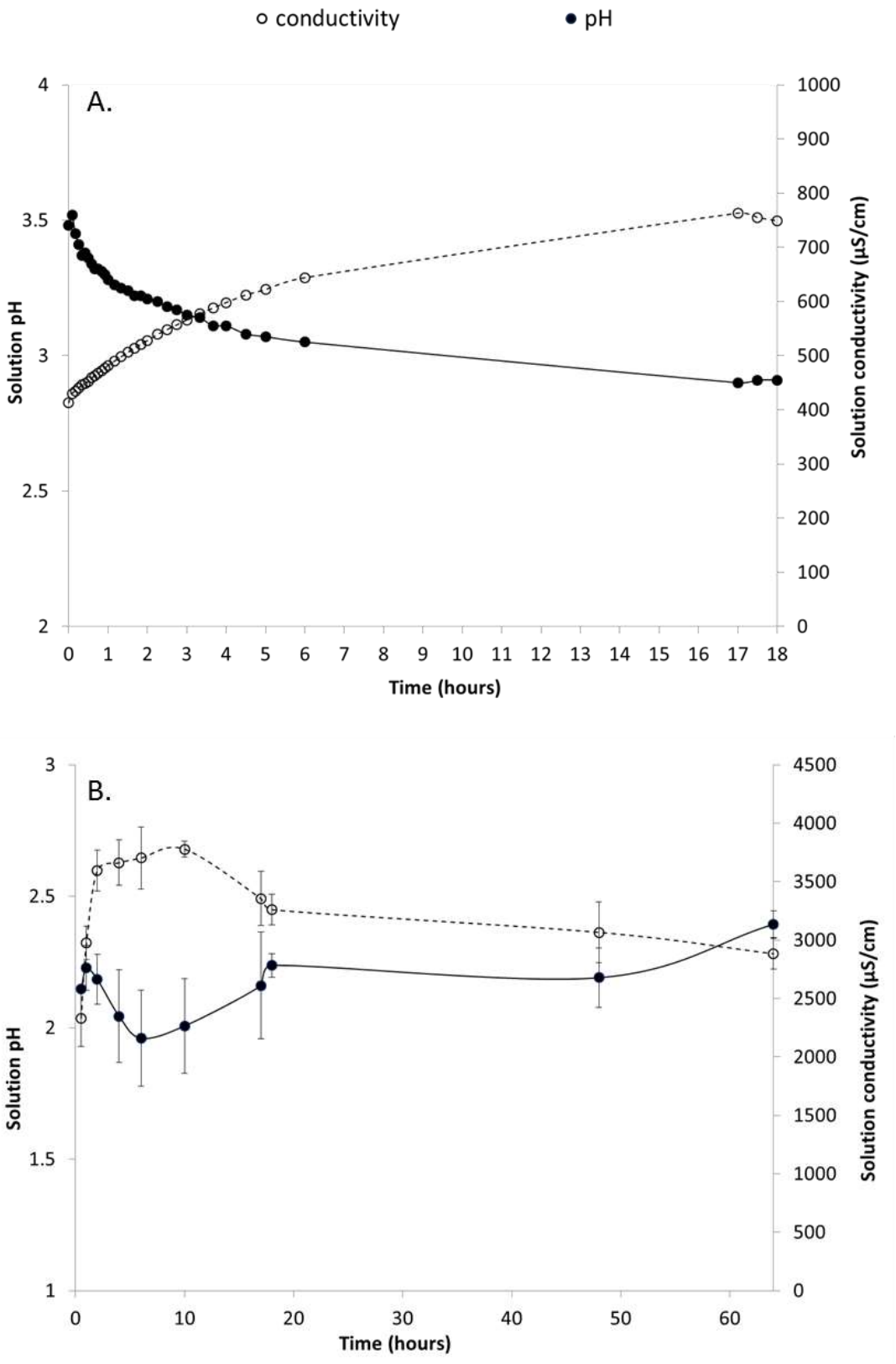

Figure 3. Changes in solution pH (closed symbol; primary y-axis) and conductivity (open symbol; secondary y-axis) during dissolution of MT_{tct} ($MT_{45\text{-}75}$: $(NH_4)_2SO_4$ of 2:6; 550°C; 45 min) at 25°C (A) and 80°C (B) under uncontrolled pH conditions (3 g/500ml; ultra-pure water; 850 rpm) over time.

and air-drying was amorphous to XRD, was concentrated in Fe and S (SEM-EDS; result not shown), and formed at pH as low as 2. It may have been a precursor to a poorly crystalline oxyhydroxysulfate of iron, such as schwertmannite (ideal formula $Fe_8O_8(OH)_6SO_4.nH_2O$), which is a common Fe(III) precipitate identified in acid mine drainage (AMD) effluents (Bigham and Nordstrom, 2000) and acidic mine pit lakes (Santofimia et al., 2015). Alternatively, it may have been a precursor to one of the several crystalline Fe sulphate precipitates which may be found in AMD systems (See Table 1 in Majzlan, 2010).

3.4.2. Dissolution in HNO_3 solution

Secondary precipitation of Fe observed when MT_{tct} had been dispersed in water under uncontrolled pH condition at 80°C prevented the quantification of the efficiency of the thermochemical treatment for elemental extraction, in particular for Fe. For this reason, dissolution experiments under

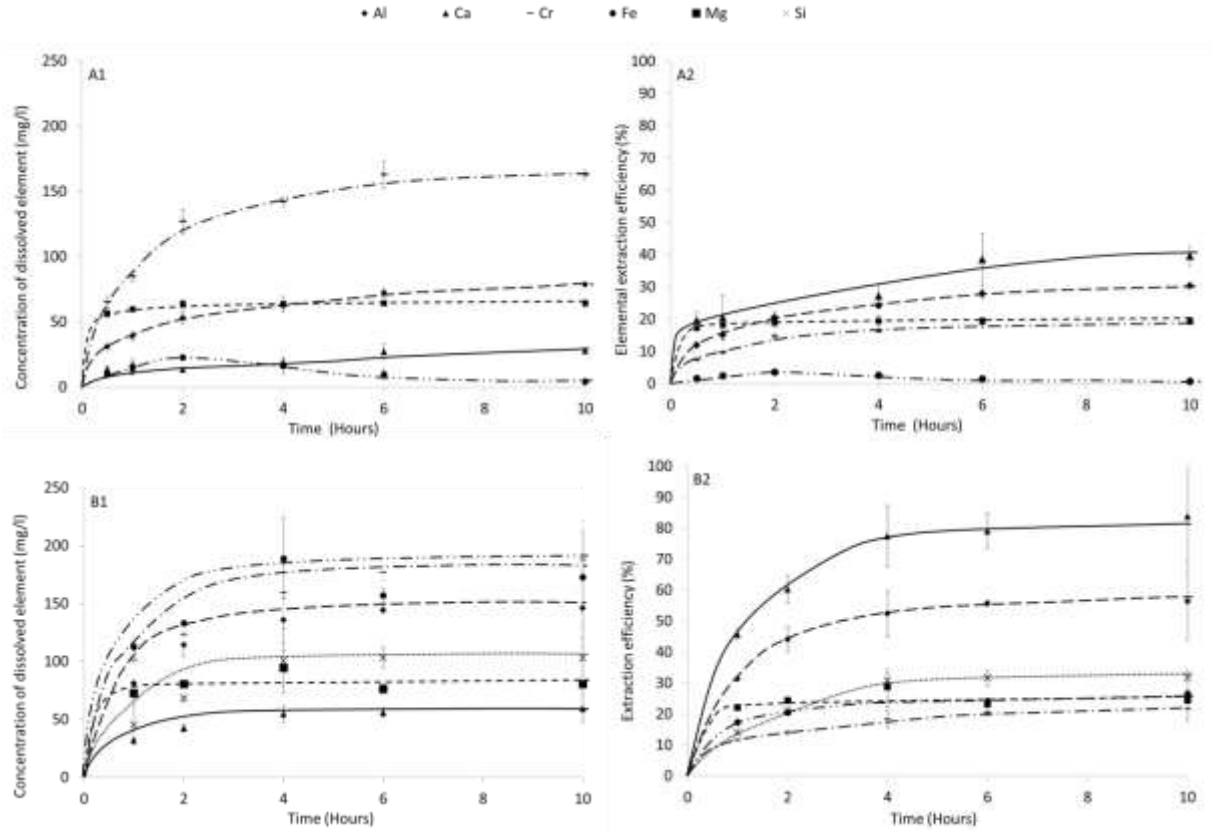

Figure 4. Changes in dissolved elemental concentration (A1, B1) and corresponding elemental extraction efficiency (A2, B2) after dissolution under uncontrolled (A.; ultrapure water) and controlled (B.; 0.63M HNO_3) pH conditions (3g MT_{tct}/500ml; 80^{o}C; 850 rpm; *n* = 2) of MT_{tct} ($MT_{45\text{-}75}$: $(NH_4)_2SO_4$ of 2:6; 550^{o}C; 45 min). Legend: Closed diamond: Al; Closed triangle: Ca; Long dash: Cr; Closed circle: Fe; Closed square: Mg; Cross: Si.

controlled acidic condition (0.63M HNO_3 solution) at the same temperature were performed to prevent secondary mineral precipitation, and to enable complete metal extraction from formed sulphate species present in MT_{tct}. During acid leaching, the suspension turned blue-grey in colour, and the non-occurrence of a brown suspension suggested that no Fe secondary precipitation had taken place under these conditions. After filtration, the solution exhibited a blue hue, which was most probably caused by the presence of soluble metal complexes. Dissolution under acid condition improved the extent of elemental extraction (Figures 4B1 and 4B2), although not to the same degree for all elements (Figures 4A2 and 4B2). For instance, the extraction efficiency for Cr and Mg increased by only 16% and 20% respectively, compared to that for Al (87%) and Ca (110%) which increased significantly. This indicated significant differences in the solubility of formed metal sulphate reaction products. Our process extracted up to 25% Mg, which is significantly better than Mg extraction efficiencies obtained for other PGM tailings using HCl leaching (Meyer et al., 2014). Up to 26% Fe and 32% Si were also extracted from the tailings. Most of Mg had dissolved within 1h of leaching, regardless of the pH conditions tested, which is the duration of dissolution used elsewhere for the recovery of metals from serpentinite (Romão et al., 2015). In our study, dissolution of other major elements was slower, with 6h being required for elemental extraction efficiency to reach or approach a plateau under acid leaching condition. After 6h dissolution, the mass of undissolved material (MT_{res}) corresponded to 52% of the starting mass of MT_{tct} (Figure 5), or 58% of the mass of untreated $MT_{45\text{-}75}$ subjected to thermochemical treatment. Decreasing the dissolution temperature below 80°C caused a substantial reduction in extraction efficiency for all elements, whereas increasing it to 95°C had a significant positive effect on Fe and Cr extraction, no effect on Ca and Si extraction (Figure 6), and enhanced the mass loss to 50%. Sulphur content analyses (S = 0.03%), TGA and XRD (results not shown) of MT_{res} confirmed the absence of metal sulphates in the non-dissolved residue generated at 95°C, which demonstrates that total metal sulphate dissolution had been achieved at this temperature. Therefore, the optimal dissolution procedure consisted of leaching MT_{tct} in 0.63M HNO_3 solution at 95°C for 6h.

FE-SEM images of received tailings ($MT_{45\text{-}75}$) revealed that the sample was made up of individual, irregularly-shaped particles with varying sizes (Figure 7A). The particles were characterized by a smooth surface topography at the scale of observation allowed by the FE-SEM, regardless of the particle size. On the other hand, MT_{tct} exhibited very different features. It consisted of unreacted, irregularly-shaped, smooth particles, surrounded by numerous newly-formed, well-defined hexagonal structures that were either individual, or interlocked particles that had formed clusters of varying sizes (sub-10µm and sub-micron; Figure 7B). The hexagonal structures were

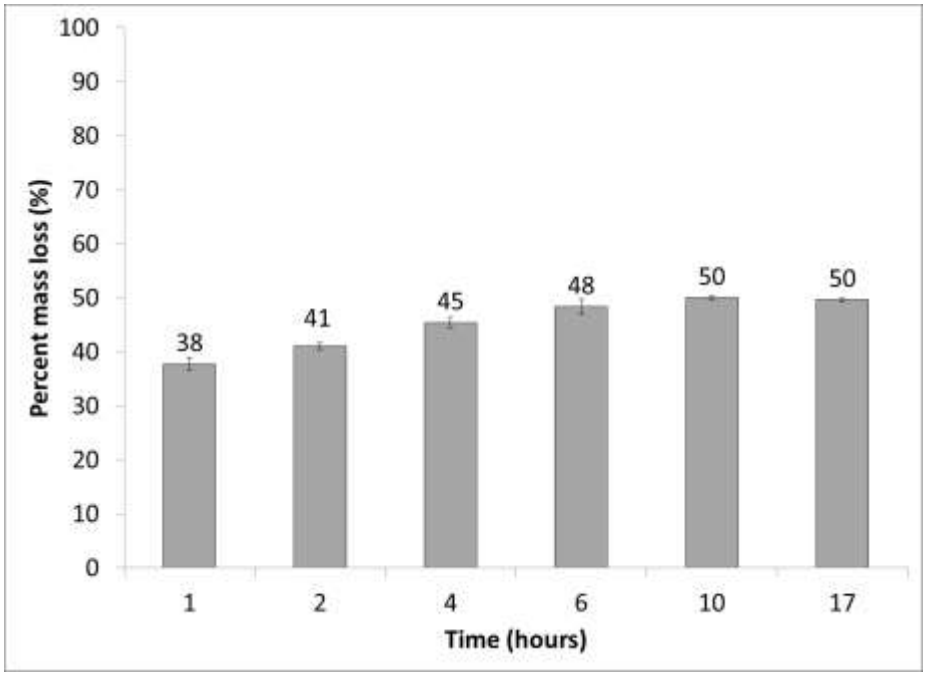

Figure 5. Experimental mass loss data as a function of leaching time for MT_{tct} ($MT_{45\text{-}75}$: $(NH_4)_2SO_4$ of 2:6; 550^oC; 45 min) dissolved in 0.63M HNO_3 (3g MT_{tct}/500ml; 80^oC; 850 rpm; *n* = 2).

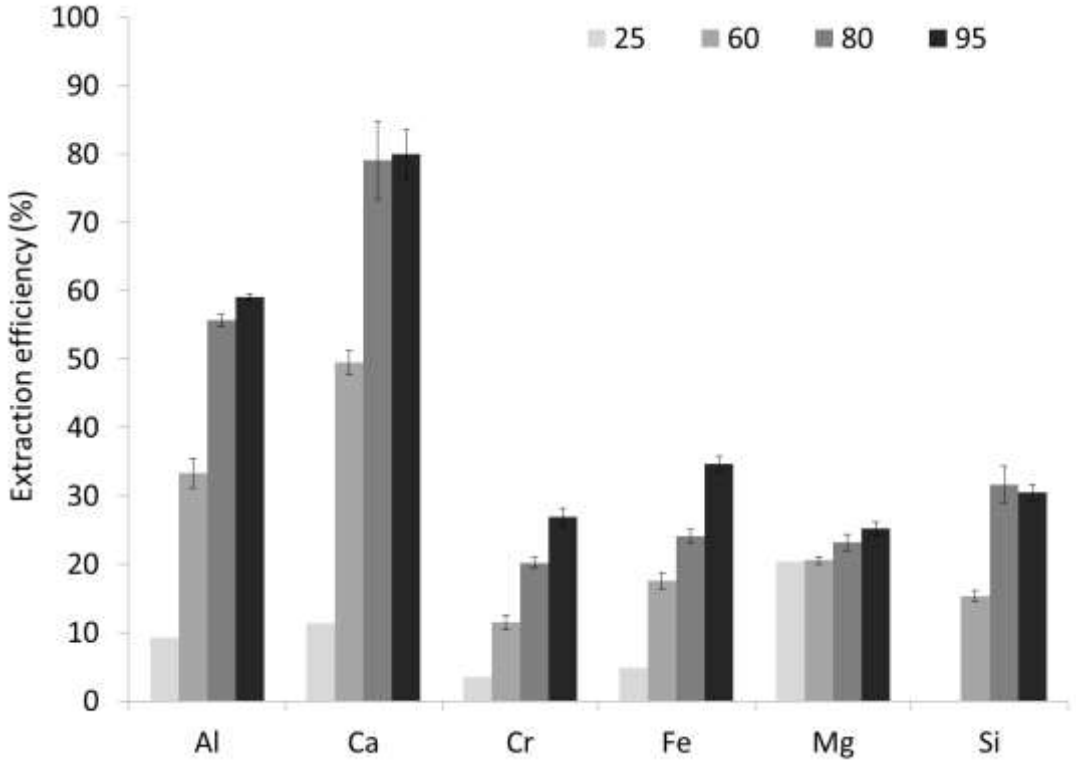

Figure 6. Elemental extraction efficiency as a function of dissolution temperature for MT_{tct} ($MT_{45\text{-}75}$: $(NH_4)_2SO_4$ of 2:6; 550^oC; 45 min) dissolved in 0.63M HNO_3 (3g MT_{tct}/500ml; 850 rpm; 6h reaction time; *n* = 2). The legend displays the dissolution temperatures.

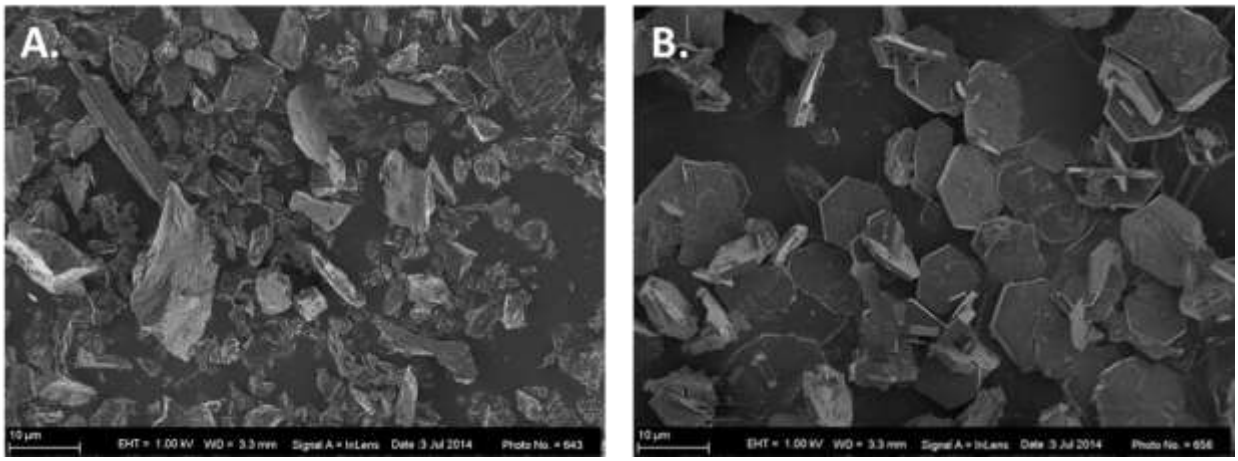

Figure 7. FE-SEM micrographs of $MT_{45\text{-}75}$ (A.; untreated) and MT_{tct} (B.; $MT_{45\text{-}75}$: $(NH_4)_2SO_4$ of 2:6; 550°C; 45 min) obtained at 18000x magnification.

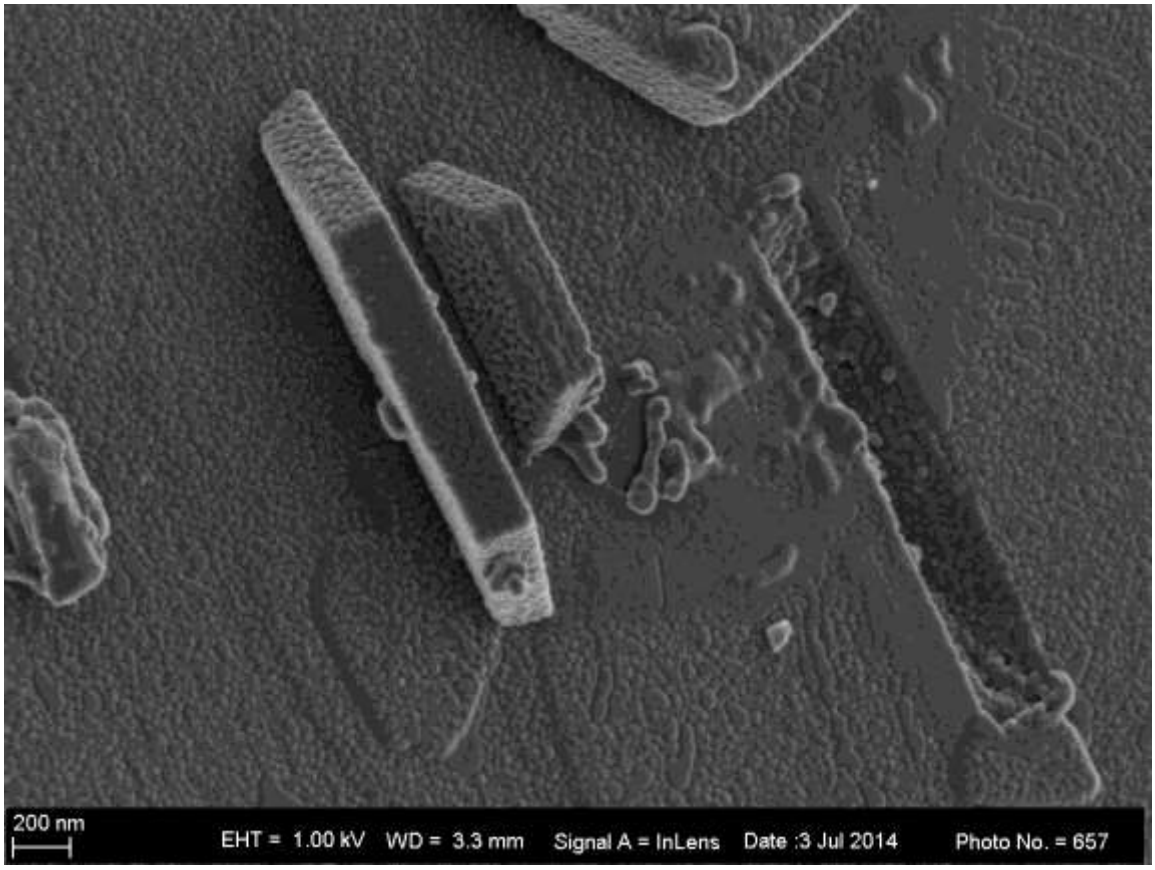

Figure 8. High-magnification (75000x) FE-SEM micrograph of a representative, hexagonally-shaped particle present in MT_{tct} (B.; $MT_{45\text{-}75}$: $(NH_4)_2SO_4$ of 2:6; 550°C; 45 min).

plate-like particles that were characterized by grainy surfaces (Figure 8). These structures were not identified in the non-dissolved residues (Figure 9) and had therefore dissolved during the leaching step. They were most probably metal (Fe, Al, Cr, and/or Mg) sulphates, since metal sulphate crystals

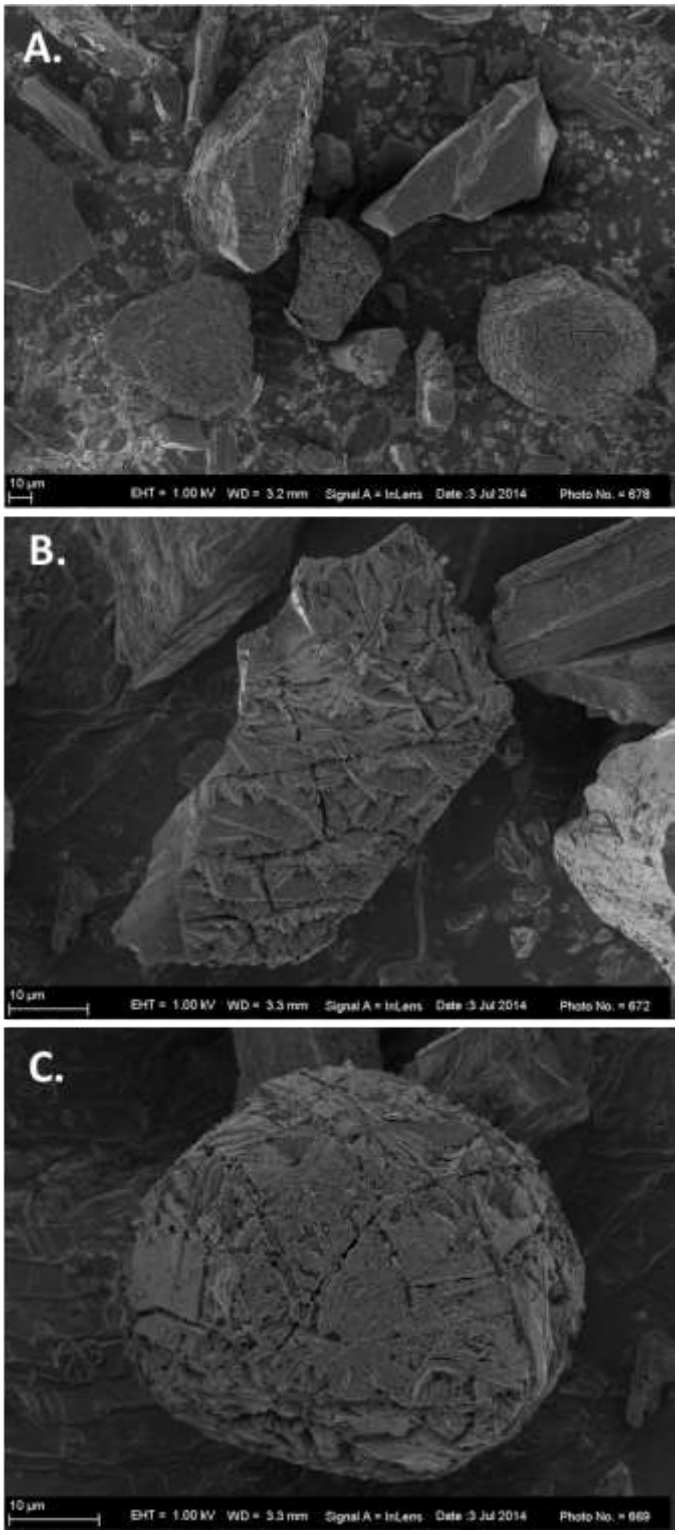

Figure 9. FE-SEM micrographs of representative particles present in non-dissolved residues (MT_{res}) generated following optimal dissolution of MT_{tct} obtained by thermochemical treatment ($MT_{45\text{-}75}$: $(NH_4)_2SO_4$ of 2:6; 550°C; 45 min). Magnifications of 1000x (A.), 3500x (B.) and 4000x (C.)

generally display hexagonal configurations (Jambor et al., 1995; Debbarma et al., 2013). The disappearance of these hexagonal particles following leaching was in agreement with XRD, which demonstrated that formed mikasaite-like structures had been identified in MT_{tct}, but not in MT_{res}. PGM tailings are characterized by a strong inter-particle variation in terms of morphology, size, and more importantly chemical and mineralogical composition. It was therefore conceivable that individual particles may have reacted with $(NH_4)_2SO_4$ in different ways and/or to varying extent during the solid-solid thermochemical treatment. For instance, a number of particles appeared to have remained intact following thermochemical treatment (Figure 9A), while others were deeply partially etched, exposing surfaces with very distinct features (Figures 9B and 9C). The micrographs suggested that some particles may have acted as nucleating surfaces for hexagonal crystal formation and growth. The leaching step may have dissolved these hexagonal structures, which probably left deep etching marks as those observed at the surface of treated tailings particles. The occurrence of numerous etched particles with nearly spherical shapes (Figure 9C) could not be explained at this stage.

4 Process implications

There are currently no known commercial processes for the extraction of major elements from PGM tailings. Such elements may include aluminium, iron, magnesium and calcium. In South Africa where no mineable bauxite deposits are available for the supply of aluminium, solid residues such as coal fly ash and PGM tailings may represent suitable alternatives to aluminium import. The country is also deprived of onshore geological reservoirs with standard properties for carbon capture and storage (Cloete, 2010); PGM tailings are concentrated in magnesium, which could be converted to magnesite in the context of CO_2 mineralization (Doucet, 2011; Vogeli et al., 2011; Amponsah-Dacosta and Reid, 2014). Regarding the supply of iron, South Africa contributes a mere 0.8% of the global iron ore reserves (Mohale et al., 2015). Geological formations of the BIC contain moderate concentrations of iron, implying that tailings from BIC mining can offer secondary sources of the metal.

The sulphuric acid method for treating South African chromite ore requires the use of highly concentrated acid (≥ 80% wt) at elevated temperature (Jiang et al., 2014), which is associated with the needs of a highly corrosive environment and of the disposal of concentrated used acid. In contrast, the process described here uses dilute acid to dissolve the metallic elements, and the dissolution takes place at temperatures below 100^{o}C. It also makes uses of $(NH_4)_2SO_4$ as low-cost extracting agent, which can subsequently be recycled. However, both the acid leaching method and

the thermochemical method suffer from a lack of elemental selectivity, with several metals having a chemical affinity with sulphate being co- extracted. Although the studied process is promising as an alternative to strong inorganic acid leaching, it requires detailed investigation of the mechanisms involved as well as optimization of the key parameters that drive the extraction process.

5 Conclusions

The potential for extracting major elements from PGM tailings was demonstrated in this study. While major elements generally represent low-value metals, they also represent the bulk composition of minerals present in tailings. It was therefore important to confirm that thermochemical treatment using a widely available, low-cost, recyclable extracting agent can improve the reactivity and dissolution behaviour of minerals contained in tailings for elemental extraction. $(NH_4)_2SO_4$ was shown to represent a promising extracting agent. Its use during thermochemical processing of tailings increased the extraction efficiencies of aluminium from 0% to ca. 60%, calcium from 4% to ca. 80%, iron from 0% to ca. 35%, chromium from 0% to ca. 27%, and magnesium from 0.6% to 24%. The process was not element-selective, and the chemical affinity between $(NH_4)_2SO_4$ and major elements under thermal conditions led to the formation of several water-soluble sulphate-metal species. This extraction process offers the significant advantage of recovering major elements from tailings in a readily-available soluble form, which could be subsequently converted to value-added products. The latter could enable the economical usage and therefore viability of PGM mine tailings management via valorisation. All the envisaged modes of use of the tailings could significantly reduce the volumes of tailings, and could contribute to the sustainability of the mining sector and to reduction of penalties imposed on mines for waste accumulation.

Acknowledgments

This work is based on research supported by the Council for Geoscience, the South African Department of Mineral Resources (DMR), the University of Pretoria, and the Geological Society of South Africa (GSSA) Ante the GSSA REI Fund. S.M. was supported by a Masters' Block Grant Free Standing Scholarship from the National Research Foundation of South Africa (NRF). Any opinion, finding, conclusion or recommendation expressed in this material is that of the authors and the NRF does not accept any liability in this regard.

References

Abd-Elzaher, M.M. (1999) Investigation of the reaction of roasted serpentine ore with some ammonium salts. Journal of the Chinese Chemical Society 46, 975-982.

African Rainbow Minerals. (2013). Integrated annual report. [ONLINE] Available at: http://www.arm.co.za/im/r_annual.php. [Accessed 14 August 2014].

Amponsah-Dacosta, M., Reid, D.L. (2014). Mineralogical Characterization of Selected South African Mine Tailings for the Purpose of Mineral Carbonation. In: An Interdisciplinary Response to Mine Water Challenges. Sui Sun & Wang (eds), China University of Mining and Technology Press, Xuzhou, China, pp. 686-689.

Anglo Platinum (2009) Annual Sustainability Report. Anglo Platinum Ltd (AP), Johannesburg, South Africa, Years 2002 to 2009, www.angloplats.com.

Asif, Z., Chen, Z. (2016) Environmental management in North American mining sector. Environmental Science and Pollution Control 23, 167-179.

Bayer, G., Kahr, G., Mueller-Vonmoos, M. (1982). Reactions of aluminium sulphates with kaolinite and other silicate and oxide minerals. Clay Minerals 17, 271-283.

Bigham, J.M., Nordstrom, D.K. (2000). Iron and aluminum hydroxysulfates from acid sulphate waters. In: Sulfate Minerals – Crystallography, Geochemistry and Environmental Significance. Rev. Min. Geochem., vol. 40, eds. C.N. Alpers, J.L. Jambor, D.K. Nordstrom, Mineralogical Society of America, Washington DC, 352-403.

Cawthorn, R.G., Eales, H.V., Walraven, F., Uken, R., Watkeys, M.K. (2006). The Bushveld Complex, In: Johnson, M.R., Anhaeusser, C.R., Thomas, R.J. (Eds.), The Geology of South Africa; Geological Society of South Africa, Johannesburg, Council for Geoscience, Pretoria, 261-281.

Chmielewski, A.G., Wawszczzak, D., Brykala, M. (2016) Possibility of uranium and rare metal recovery in the Polish copper mining industry. Hydrometallurgy 159, 12-18.

Cloete, M. (2010) Atlas on geological storage of carbon dioxide in South Africa. Council for Geoscience.

Debbarma, M., Das, S., Saha, M. (2013) Effect of reducing agents on the structure of zinc oxide under microwave irradiation. Advances in Manufacturing 1, 183-186.

De Beer, M., Maree, J.P., Liebenberg, L., Doucet, F.J. (2014). Conversion of calcium sulphide to calcium carbonate during the process of recovery of elemental sulphur from gypsum waste. Waste Management 34, 2373-2381.Dixon, P. (1944) Formation of Sulphamic Acid during the Thermal Decomposition of Ammonium Sulfate. Nature 154, 706.

Doucet, F.J. (2011) Scoping study on CO_2 mineralization technologies. Contract Report No CGS-2011-007, commissioned by the South African Centre for Carbon Capture and Storage, pp.88.

Eales, H.V. (2014). The Bushveld Complex, an introduction to the geology and setting of the Bushveld Complex. Council for Geoscience, 214pp.

Fagerlund, J., Nduagu, E., Romão, I., Zevenhoven, R. (2012) CO_2 fixation using magnesium silicate minerals Part 1: Process description and performance. Energy 41, 184-191.

Frändegård, P., Krook, J., Svensson, N. (2015) Integrating remediation and resource recovery: on the economic conditions of landfill mining. Waste Management 42, 137-147.

Gehrke, I., Geiser, A., Somborn-Schulz, A. (2015) Innovations in nanotechnology for water treatment. Nanotechnology, Science and Applications 8, 1-17.

Ghacham, A.B., Cecchi, E., Pasquier, L.C., Blais, J.F., Mercier G. (2015) CO_2 sequestration using waste concrete and anorthosite tailings by direct mineral carbonation in gas-solid-liquid and gas-solid routes. Journal of Environmental Management 163, 70-77.

Gutiérrez, S.C., Coulon, F., Jiang, Y., Wagland, S. (2015) Rare earth elements and critical metal content of extracted landfilled material and potential recovery opportunities. Waste Management 42, 128-136.

Highfield, J., Lim, H., Fagerlund, J., Zevenhoven, R. (2012) Activation of serpentine for CO_2 mineralization by flux extraction of soluble magnesium salts using ammonium sulfate. RSC Advances 2, 6535-6541.

Huisamen, A. (2013). Contaminant mobilisation by fluid-rock interaction and related transport mechanisms in platinum tailings. MSc thesis, University of Pretoria, Pretoria, South Africa.

Implats (2015) Mineral resources and mineral reserves statement 2015 (http://financialresults.co.za/2015/implats-minerals-report-2015/chromium.php (accessed on 12 February 2016).

Jambor, J.L., Pertsev, N.N., Roberts, A.C. (1995) New mineral names. American Mineralogist 80, 845-850.

Jariwala, M., Crawford, J., LeCaptain, D.J. (2007) In situ raman spectroscopic analysis of the regeneration of ammonium hydrogen sulfate from ammonium sulfate. Industrial & Engineering Chemistry Research 46, 4900-4905.

Jiang, M., Zhao, Q., Liu, C., Shi, P., Zhang, B; Yang, D.; Saxen, H., Zevenhoven, R. (2014) Sulfuric acid leaching of a South African chromite. Part 2: optimization of leaching conditions. International Journal of Mineral Processing 130, 102-107.

Jubilee Platinum (2015) http://www.jubileeplatinum.com/investors-and-media/announcements/2015/15-dec-2015.php (accessed on 12 February 2016).

Kiyoura, R., Urano, K. (1970) Mechanism, kinetics and equilibrium of thermal decomposition of ammonium sulphate. Industrial & Engineering Chemistry Process Design and Development 9, 489-494.

Krook, J., Svensson, N., Eklund, M. (2012) Landfill mining: a critical review of two decades of research. Waste Management 32, 513-520.

Krouse, K.A., Badri, M. (1991) Thermal studies on chromium(II) salts. Thermochimica Acta 177, 239-251.

Lee, C.T., Sohn, H.T. (1989) Recovery of synthetic rutile and iron oxide from ilmenite ore by sulfation with ammonium sulfate. Industrial & Engineering Chemistry Research 28, 1802–1808.Li, D.X., Gao, G.L., Meng, F.L., Ji, C. (2008) Preparation of nano-iron oxide red pigment powders by use of cyanided tailings. Journal of Hazardous Materials 155, 369-377.

Liu, Y., Naidu, R. (2014) Hidden values in bauxite residue (red mud): Recovery of metals. Waste Management 34, 2662-2673.

Ma, D., Wang, Z., Guo, M., Zhang, M., Liu, J. (2014) Feasible conversion of solid waste bauxite tailings into highly crystalline 4A zeolite with valuable application. Waste Management 34, 2365-2372.

Majzlan, J. (2010) Advances and gaps in the knowledge of thermodynamics and crystallography of acid mine drainage sulphate minerals. Chimia 64, 699-704.

Meyer, N.A., Vogeli, J.U., Becker, M., Broadhurst, J.L., Reid, D.L., Franzidis, J.P. (2014) Mineral carbonation of PGM mine tailings for CO_2 storage in South Africa: a case study. Minerals Engineering 59, 45-51.

Mohale, S., Masetlana, T.R., Bonga, M., Ikaneng, M., Dlambulo, N., Malebo, L., Mwape, P. (Eds) (2015) South Africa's Mining Industry 2013-2014. Department of Mineral Resources, South Africa, pp. 276.Mohamed, S. (2015) Extraction of major elements from PGE tailings in view of nanoparticle synthesis for environmental technological application. Unpublished MSc thesis, University of Pretoria, South Africa, pp. 192.

Mudher, K.D.S., Keskar, M., Venugopal, V. (1999) Solid state reactions of CeO_2, ThO_2 and PuO_2 with ammonium sulphate. Journal of Nuclear Materials 265, 146-153.

Muthukannan, V., Praveen, K., Natesan, B. (2015) Fabrication and characterization of magnetite/reduced graphene oxide composite incurred from iron ore tailings for high performance application. Materials Chemistry and Physics 162, 400-407.

Nagaishi, T., Ishiyama, S., Matsumoto, M., Yoshinaga, S. (1984) Reactions between ammonium sulphate and metal oxides (metal=Cr, Mn and Fe) and thermal decomposition of the products. Journal of Thermal Analysis 29, 121-129.

Nduagu, E., Björklöf, T., Fagerlund, J., Wärnå, J., Geerlings, H., Zevenhoven, R. (2012) Production of magnesium hydroxide from magnesium silicate for the purpose of CO_2 mineralisation. Part 1. Application to Finnish serpentinite. Minerals Engineering 30, 75-86.

Nduagu, E.I., Highfield, J., Chen, J., Zevenhoven, R. (2014) Mechanisms of serpentine-ammonium sulphate reactions studied by coupled thermal-spectroscopic methods: Towards higher efficiencies in flux recovery and Mg extraction for CO_2 mineral sequestration. RSC Advances 4, 64494-64505.

Romão, I., Nduagu, E., Fagerlund, J., Gando-Ferreira, L.M., Zevenhoven, R. (2012) CO_2 fixation using magnesium silicate minerals. Part 2: Energy efficiency and integration with iron-and steelmaking. Energy 41, 203-211.

Romão, I., Slotte, M., Gando-Ferreira, L.M., Zevenhoven, R. (2014) CO_2 sequestration with magnesium silicates – Exergetic performance assessment. Chemical Engineering Research and Design 92, 2072-2082.

Romão, I., Gando-Ferreira, L.M., Zevenhoven, R. (2015) Separation and recovery of valuable metals extracted from serpentinite during the production of $Mg(OH)_2$ for CO_2 sequestration. Minerals Engineering 77, 25-33.

Rule, C.M. (2008). Energy considerations in the current PGM processing flowsheet utilizing new technologies. Third International Platinum Conference 'Platinum in Transformation', The Southern African Institute of Mining and Metallurgy, 45-52.

Schouwstra, R.P., Kinloch, E.D. (2000). A short geological review of the Bushveld Complex. Platinum Metals Review 44, 33-39.

Santofimia, E., López-Pamo, E., Montero, E. (2015) Selective precipitation of schwertmannite in a stratified acidic pit lake of Iberian Pyrite Belt. Mineralogical Magazine 79, 497-513.

Tagawa, H. (1984) Thermal decomposition temperatures of metal sulfates. Thermochimica Acta 80, 23-33.

Vandenberghe, R.E., de Resende, V.G., da Costa, G.M., De Grave, E. (2010). Study of loss-on-ignition anomalies found in ashes from combustion of iron-rich coal. Fuel 89, 2405-2410.

Vogeli, J., Reid, D.L., Becker, M., Broadhurst, J., Franzidis, J.-P. (2011). Investigation of the potential for mineral carbonation of PGM tailings in South Africa. Minerals Engineering 24, 1348-1356.

Wagner, T.P., Raymond, T. (2015) Landfill mining: Case study of a successful metals recovery project. Waste Management 45, 448-457.

Watson, G.V.R., Stringfellow, A.M., Powrie, W., Turner, D.A., Coello, J. (2016) Solid waste systems assessment. In: The future of national infrastructure (Eds. J.W. Hall, M. Tran, A.J. Hickford, R.J. Nicholls). Chapter 8, Cambridge University Press, UK.

Xiao, J., Li, F., Zhong, Q., Bao, H., Wang, B., Huang, J., Zhang, Y. (2015) Separation of aluminum and silica from coal gangue by elevated temperature acid leaching for the preparation of alumina and SiC. Hydrometallurgy 155, 118-124.

Supplementary Figure

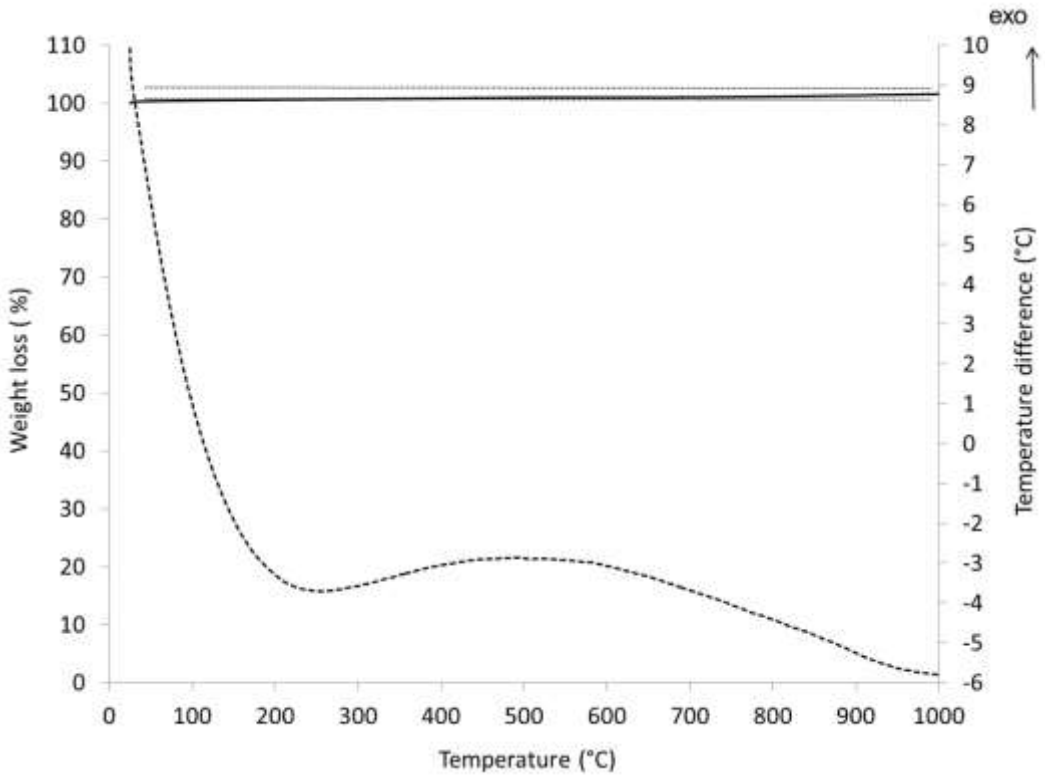

Figure S1. TGA and DTA curves of untreated $MT_{45\text{-}75}$.